Molecular Pharmacology Fast Forward. Published on December 17, 2020 as DOI: 10.1124/molpharm.120.000129
This article has not been copyedited and formatted. The final version may differ from this version.

1. Title page

Insights into the structure-activity relationship of glycosides as positive allosteric modulators acting on P2X7 receptors

Waraporn Piyasirananda, Andrew Beekman, A. Ganesan, Stefan Bidula, Leanne Stokes

School of Pharmacy, University of East Anglia, Norwich Research Park, Norwich UK.

Conflict of interest:

The authors declare that there is no conflict of interest.

Molecular Pharmacology Fast Forward. Published on December 17, 2020 as DOI: 10.1124/molpharm.120.000129
This article has not been copyedited and formatted. The final version may differ from this version.

Running title: P2X7 positive modulator SAR

Corresponding author address:

Dr Leanne Stokes, School of Pharmacy, University of East Anglia, Norwich Research Park, Norwich NR4 7TJ, UK.

Telephone: +44 1603 592403

Email: l.stokes@uea.ac.uk

Text pages: 29

Number of Tables: 1

Number of Figures: 8

Number of references: 38

Word counts:

Abstract: 247

Introduction: 411

Discussion: 1480

Non-standard abbreviations:

PAM; positive allosteric modulator

Molecular Pharmacology Fast Forward. Published on December 17, 2020 as DOI: 10.1124/molpharm.120.000129
This article has not been copyedited and formatted. The final version may differ from this version.

3. Abstract

P2X7 is an important ligand-gated ion channel expressed in multiple immune cell populations. This study aimed to investigate the chemical requirements of triterpenoid glycosides within a new binding pocket to characterise the structure-activity relationship. A set of glycosides were screened for positive modulator activity at human P2X7 using a YO-PRO-1 dye uptake assay in HEK-hP2X7 cells. The highest positive modulator activity was with ginsenoside CK, containing a monosaccharide (glucose) attached at carbon-20. Ginsenoside 20(*S)*Rg3, containing a disaccharide group (glucose-glucose) at carbon-3, displayed positive modulator activity with a reduced EC_{50} for ATP and increased maximal response at hP2X7. The epimer 20(*R)*Rg3 was inactive. A similar stereo-specific pattern was observed for 20(*S)*-Rh2. Ginsenoside-F1, highly similar to ginsenoside CK but containing a single additional hydroxyl group, was also inactive at P2X7. Computational docking suggests hydrophobic residues in the pocket are involved in steric discrimination between triterpenoids, while the position and identity of the carbohydrate group is important for positive modulator activity at human P2X7. Ginsenosides containing monosaccharide attachments perform better than di- or tri-saccharide glycosides. Additional modifications to the triterpenoid scaffold at carbon-6 are not tolerated. Gypenosides from plant sources other than *Panax ginseng* (gypenoside XVII, gypenoside XLIX, stevenleaf) can also act as positive allosteric modulators of P2X7. We also investigated the effect of positive allosteric modulators on endogenous P2X7 in THP-1 monocytes and confirmed our findings in a calcium response assay. A cell viability assay showed potentiation of ATP-induced cell death with ginsenoside CK in THP-1 and HEK-hP2X7 cells.

Keywords: P2X7, ginsenoside, positive allosteric modulator, ATP

Molecular Pharmacology Fast Forward. Published on December 17, 2020 as DOI: 10.1124/molpharm.120.000129
This article has not been copyedited and formatted. The final version may differ from this version.

4. Significance statement

Ginsenosides are active as PAMs at P2X7 and this study determines the chemical features important for mediating this effect. The position and identity of the sugar group is important for activity as is the position of a number of hydroxyl groups on the triterpenoid scaffold. Diastereomers of ginsenosides Rg3 and Rh2 demonstrate the importance of the location of hydroxyl groups relative to the hydrophobic face of the predicted binding pocket.

Molecular Pharmacology Fast Forward. Published on December 17, 2020 as DOI: 10.1124/molpharm.120.000129
This article has not been copyedited and formatted. The final version may differ from this version.

Introduction

The ligand-gated ion channel P2X7 is important in regulating immune cell responses during infection and inflammation (Di Virgilio et al., 2017). In particular, P2X7 is a known physiological regulator of the NLRP3-caspase 1 inflammasome complex and controls the secretion of pro-inflammatory cytokines such as IL-1β and IL-18 (Giuliani et al., 2017). Many studies have demonstrated that activation of P2X7 in infected macrophages *in vitro* can promote microbial killing. Intracellular bacteria and parasites such as *Mycobacterium tuberculosis* (Fairbairn et al., 2001, Placido et al., 2006), *Toxoplasma gondii* (Moreira-Souza et al., 2017) and *Leishmania amazonensis* (Chaves et al., 2014) are examples of pathogens where P2X7 contributes to microbicidal mechanisms. *In vivo* mouse models of infection suggest that global deficiency in P2X7 can affect pathogen burden and inflammation (Miller et al., 2015, Chaves et al., 2019). Furthermore, inheritance of loss-of-function variants of human P2X7 have been linked to susceptibility to infections and complications such as extra-pulmonary TB (Areeshi et al., 2015, Fernando et al., 2007). Development of a positive allosteric modulator (PAM) of P2X7 may therefore be useful in treatment of such infections (Stokes et al., 2020). This type of therapy directed at enhancing host responses would reduce the need for antibiotics and be beneficial in avoiding development of antibiotic resistance.

Triterpenoid glycosides from *Panax ginseng* have PAM activity at human P2X7 with the *in vivo* metabolite ginsenoside compound K (CK) demonstrating the highest activity (Helliwell et al., 2015). Using a combination of computational docking and mutagenesis, we previously characterised a novel binding pocket for ginsenosides within the central vestibule of human P2X7 (Bidula et al., 2019b). Predicted binding poses identified two modes of binding dependent on the carbohydrates attached to the ginsenoside in question. Ginsenoside CK contains a single carbohydrate (glucose) moiety which makes multiple contacts with amino acids Asp318, Leu320 and Ser60. Conversely, ginsenoside Rd contains both disaccharide (-glucose-glucose) and monosaccharide glucose moieties and is predicted

Molecular Pharmacology Fast Forward. Published on December 17, 2020 as DOI: 10.1124/molpharm.120.000129
This article has not been copyedited and formatted. The final version may differ from this version.

to use the disaccharide moiety for binding to P2X7 (Bidula et al., 2019b). The presence of carbohydrate moieties is deemed essential for PAM activity since the aglycone protopanaxadiol has no activity at P2X7 (Helliwell et al., 2015).

In this study, we explored the chemical structural requirements of triterpenoid glycosides with the aim of building a structure-activity relationship for positive modulators at P2X7. This revealed critical information about the tolerance of substitutions at C-6 and the preference for glucose as the attached sugar moiety. This provides important knowledge for the future development of selective PAMs for P2X7.

Molecular Pharmacology Fast Forward. Published on December 17, 2020 as DOI: 10.1124/molpharm.120.000129
This article has not been copyedited and formatted. The final version may differ from this version.

Materials and Methods

Materials

Ginsenoside CK (CAS 39262-14-1), ginsenoside-Rb1 (CAS 41753-43-9), ginsenoside-Rd (CAS 52705-93-8), 20(*S)*-ginsenoside-Rg3 (CAS 14197-60-5), 20*(R)*-ginsenoside-Rh2 (CAS 112246-15-8), protopanaxadiol (PPD) (CAS 30636-90-9), glycyrrhizic acid (CAS 1405-86-3), stevioside (CAS 57817-89-7), daucosterol (CAS 474-58-8), esculentoside A (CAS 65497-07-6), mogroside V (CAS 88901-36-4), saikosaponin A (CAS 20736-09-8), stevenleaf (CAS 80321-63-7) were from Shanghai Richem International Ltd, China (supplier code CDCMANSETE). Ginsenoside CK (CAS 39262-14-1), ginsenoside-F2 (CAS 62025-49-4), ginsenoside-F1 (CAS 53963-43-2), gypenoside XLIX (CAS 94987-08-3), gypenoside XVII (CAS 80321-69-3), 20*(S)*-ginsenoside-Rg3 (CAS 14197-60-5), 20*(R)*-ginsenoside -Rg3 (CAS 38243-03-7), 20*(S)*-ginsenoside-Rh2 (CAS 78214-33-2), 20*(R)*-ginsenoside-Rh2 (CAS 112246-15-8) were from ChemFaces (Wuhan Chemfaces). Scilliroside (CAS 507-60-8, NSC7523), ouabain (CAS 630-60-4, NSC25485), solanine hydrochloride (CAS 20562-02-1, NSC35611), solasonine (CAS 19121-58-5, NSC82149) were obtained from the NCI DTP chemical repository. ATP (Sigma-Aldrich, A7699) was dissolved in distilled water to 100 mM and adjusted to pH 7.4 with 5 M NaOH. Aliquots of ATP were kept frozen at -20 °C and used once in experiments. AZ10606120 (CAS 607378-18-7, Tocris Biosciences) and AZ11645373 (CAS 227088-94-0) Sigma-Aldrich) were dissolved in DMSO to 10 mM and stored at -20 °C. Fura-2AM (CAS 108964-32-5, HelloBio) was prepared in DMSO to a concentration of 1 mM, aliquoted, and stored at -20 °C in amber-coloured Eppendorf vials. Sulfinpyrazone (CAS 57-96-5, Sigma Aldrich) was dissolved in methanol at a stock concentration of 25 mM and stored at +4 °C.

Molecular Pharmacology Fast Forward. Published on December 17, 2020 as DOI: 10.1124/molpharm.120.000129
This article has not been copyedited and formatted. The final version may differ from this version.

Cell culture

HEK-293 cells stably expressing the wild-type human P2X7 variant (HEK-hP2X7) were maintained in DMEM:F12 media (ThermoFisher Scientific, Life Technologies catalogue number 11320-074) containing 10% foetal bovine serum (Gibco catalogue number 10500-064) and penicillin/streptomycin (ThermoFisher Scientific) as described previously (Helliwell et al., 2015). HEK-293 cells were passaged twice weekly using 0.5% trypsin-EDTA (ThermoFisher Scientific). THP-1 human monocytic cells (a kind gift from Professor Maria O'Connell, University of East Anglia) were maintained in RPMI 1640 media (Fisher Scientific, Life Technologies catalogue number 21875-034) containing 10% foetal bovine serum (Gibco, as before) and penicillin/streptomycin (ThermoFisher Scientific). Cells were kept in a humidified incubator at 37 °C with a constant supply of 5% CO_2.

YO-PRO-1 dye uptake screening assay

ATP-induced dye uptake experiments were performed as described previously (Bidula et al., 2019b). Briefly, HEK-hP2X7 cells were plated at 2 x 10^4 cells/well (100 µl per well) in complete media and left overnight to attach to poly-D-lysine coated 96-well plates. YO-PRO-1 iodide was prepared in a low divalent buffered solution (145 mM, 2mM KCl, 13 mM D-glucose, 10 mM HEPES, 0.2 mM $CaCl_2$ pH 7.3) to a final concentration of 2 µM. Media was removed from the plate using a manual multi-channel pipette and YO-PRO-1 buffer applied to wells (180 µl per well). AZ10606120 (10 µM) was prepared in YO-PRO-1 low divalent buffer and added directly to the cells to block P2X7 by pre-treatment. A Flexstation 3 plate reader (Molecular Devices, Sunnyvale, CA, USA) was used to record YO-PRO-1 fluorescence in HEK-hP2X7 for 300 seconds following the addition of ATP (at 10X final concentration) with/without ginsenoside compounds or vehicle (DMSO). Plates were allowed to warm up to 37 ˚C for 10 minutes before initiating the recording. Baseline recordings were made for 40 seconds before compound addition using the Flexstation 3 fluidics system. YO-

Molecular Pharmacology Fast Forward. Published on December 17, 2020 as DOI: 10.1124/molpharm.120.000129
This article has not been copyedited and formatted. The final version may differ from this version.

PRO-1 fluorescence was measured at 520 nm following excitation at 490 nm (auto cut-off at 495 nm) and the sample interval was 3.5 seconds. Flexstation settings were PMT medium, 6 reads/well, pipette height 170, and a rate of injection of 3. Data was acquired using Softmax Pro v5.4 (Molecular Devices, Sunnyvale, CA, USA). To analyse the data, area under the dye uptake curve (AUC) was calculated in Softmax Pro v5 using zero baseline data with a lag time of 50 seconds (50-300 seconds).

Fura-2 calcium measurements

THP-1 cells were pelleted by centrifugation (300 *g*, 5 mins), washed and re-suspended in Hanks Balanced Salt Solution (HBSS) buffer containing 2 μM fura-2AM and 250 μM (±)-sulfinpyrazone. Cells were loaded for 1 hour in a waterbath at 37 °C while shielded from light with foil. Loaded cells were washed once with 5 ml HBSS to remove excess fura-2AM dye. THP-1 cells were then re-suspended, counted and plated at 2 x 10^5 cells/well in a standard clear 96–well plate (Thermo Scientific, NUNC 167008) in low divalent assay buffer without Mg^{2+} (145 mM NaCl, 2 mM KCl and 2 mM $CaCl_2$, 13 mM glucose, 10 mM HEPES, pH 7.3) containing 250 μM (±)-sulfinpyrazone. The 10X concentration of agonist (ATP) was prepared in the same assay buffer. ATP was injected automatically into wells at 30 seconds in a Flexstation 3 microplate reader. Ratiometric data was acquired using 340 nm and 380 nm for excitation wavelengths and 520 nm as the emission wavelength; six reads per well (PMT medium). Area under the curve (AUC) was calculated using standard zero baseline normalisation with a lag time 0-300 seconds using SoftMax Pro v5.4 software.

Cell viability assay

HEK-hP2X7 or THP-1 cells were seeded at 5 x 10^3 cells/well in a volume of 100 μL for 24 hours in 96–well plates (Thermo Scientific Nunclon Edge plates, catalogue number 167425).

Molecular Pharmacology Fast Forward. Published on December 17, 2020 as DOI: 10.1124/molpharm.120.000129
This article has not been copyedited and formatted. The final version may differ from this version.

Cells were plated in DMEM:F12 media or RPMI 1640 media containing 1% FBS and penicillin/ streptomycin for 24 hours in a humidified incubator at 37 °C with a supply of 5% CO_2. Edge wells of the plates were filled with autoclaved distilled water to prevent evaporation from wells containing cells. The compounds and ATP were made at 2X final concentration in 1% FBS DMEM:F12 media and 100 μL added to the cells for 24 hours. Following incubation, resazurin sodium salt (CAS 62758-13-8; Sigma Aldrich) at 0.1 mg/ml in sterile PBS was added to the plate (20 μl into 200 μl culture media per well). Cells were incubated for a further 2 hours in a humidified incubator at 37 °C with a supply of 5% CO_2. A Flexstation 3 microplate reader was used to acquire data. End-point fluorescence data was measured using 570 nm excitation wavelength, 600 nm emission wavelength (cut-off at 590 nm), 3 reads/well (PMT low). Data were analysed by performing background correction through subtracting blank media readings (without cells) from all samples and then normalising each sample to media treated cells (control treatment, 100%) as percentage of control.

Computational docking

The homology model of human P2X7 generated previously in (Bidula et al., 2019b) was used for docking runs using the Schrodinger Maestro suite. Three-dimensional models of ginsenoside-F1 and ginsenoside 20*(S)*-Rg3 were generated using LigPrep software and the OPLS3 force field was used to generate up to 32 low-energy conformers for each ligand. Induced-fit docking was performed using the automated extended sampling protocol, first performing several initial docking runs where side chains were either trimmed or van der Waals potentials softened according to their flexibility, then side chains were re-built and those within 5 Å of the ligand were optimised using Prime software (Jacobson et al., 2004). Structures within 30 kcal mol^{-1} of the lowest energy structure were retained. Ligands were then re-docked to the new receptor structure using the Glide SP algorithm (Friesner et al., 2004) and standard potentials. The receptor grid was centred on the highest scoring

Molecular Pharmacology Fast Forward. Published on December 17, 2020 as DOI: 10.1124/molpharm.120.000129
This article has not been copyedited and formatted. The final version may differ from this version.

potential binding site using SiteMap (Halgren, 2007) and this had a cubic box with dimensions of 30 Å. For each ginsenoside the resulting poses were clustered by heavy atom RMSD using the average-linkage method, and a representative structure was chosen from the model closest to the centroid of the most populated cluster. For ginsenoside-F1 and 20*(S)*-Rg3 the most populated cluster made up 31% and 62% of all solutions respectively.

Data and Statistical analysis

Results are expressed as mean ± SD from the indicated number of experiments. For YO-PRO-1 dye uptake and intracellular calcium experiments each independent experiment used triplicate wells and the mean of the replicates were collated and plotted. Technical replicates were used to ensure reliability of fluorescence values. Cell viability data was normalised to the vehicle control for each experiment after background correction had been performed. Dose-response curves were plotted by a non-linear regression fit with variable slope using GraphPad Prism software v7. Half maximal responses are expressed as EC_{50} values with 95% confidence intervals. These values were calculated from the collated data for each compound from three independent experiments. Statistical differences were determined by analysis of the data by one-way ANOVA followed by Dunnett's multiple comparison test or Sidak's multiple comparison test using GraphPad Prism v7. $P < 0.05$ was the accepted minimum level of significance.

Molecular Pharmacology Fast Forward. Published on December 17, 2020 as DOI: 10.1124/molpharm.120.000129
This article has not been copyedited and formatted. The final version may differ from this version.

Results

To measure positive modulator activity at human P2X7 receptors we used a well characterised HEK-hP2X7 stable cell line (Helliwell et al., 2015) and a YO-PRO-1 dye uptake assay performed on a Flexstation 3 plate reader. Figure 1A shows a typical dye uptake response to an approximate EC_{50} concentration of agonist (200 μM ATP) and the effect of co-administration of ginsenoside-CK or ginsenoside-Rd at a final concentration of 10 μM. We previously demonstrated that pre-treatment with a selective P2X7 antagonist AZ10606120 abolished the response, confirming that the effect of the ginsenosides was dependent on P2X7 activation (Helliwell et al., 2015). Dose-response experiments demonstrated that ginsenosides CK and Rd have two effects on ATP-induced responses at hP2X7 (**Figure 1B**); an increase in the maximum response (a Type I PAM effect) and a shift in the dose-response curve to the left (a Type II PAM effect), thereby enhancing the maximum effect of the agonist and reducing the EC_{50} value. Classification of Type I, Type II and Type I/II mixed PAM effects have been previously used for NMDA receptors (Hackos and Hanson, 2017) and the same naming convention for P2X receptors is discussed in a recent review (Stokes et al., 2020). Ginsenoside-CK reduced the EC_{50} for ATP to 80.2 μM compared to an average EC_{50} for ATP + vehicle (DMSO) of 219 μM (n=5 experiments) and increased the maximum response by 2.4-4.4 fold. Both ginsenoside-CK and Rd have mixed Type I/II effects. Ginsenoside-Rb1 increased the maximum response by 1.9-fold but had little effect on the EC_{50} value (175.9 μM (**Figure 1B**) and therefore has only Type I activity. The aglycone ginsenoside metabolite protopanaxadiol (PPD) had no effect on the ATP dose-response curve (**Figure 1B**).

Investigating glycosylation patterns

We assumed that the carbohydrate groups play a key role in mediating this response at P2X7 since the aglycone PPD had no effect (**Figure 1B**). Our previous study identified a

Molecular Pharmacology Fast Forward. Published on December 17, 2020 as DOI: 10.1124/molpharm.120.000129
This article has not been copyedited and formatted. The final version may differ from this version.

binding site within the human P2X7 trimeric structure based on computational docking to a homology model. The single glucose moiety on ginsenoside CK makes predicted interactions with P2X7 β-strands lining the lateral portals which connect the agonist-binding site to the ion channel transmembrane domains (Bidula et al., 2019b). We investigated the effect of varying the number of sugar moieties attached to the steroid-like scaffold by searching for chemicals similar to ginsenosides that were commercially available as purified chemicals. We excluded ginsenosides from the protopanaxatriol series with sugars attached on carbon-6 as our previous work has demonstrated these compounds to have no activity at P2X7 (Helliwell et al., 2015). We identified a number of candidate glycosides to test (**Table 1**) and screened these compounds at a final concentration of 10 μM on hP2X7 responses using a fixed concentration of ATP (200 μM) in the YO-PRO-1 dye uptake assay. Focusing on glycosides containing a disaccharide moiety first (**Figure 2**) we found that ginsenoside Rg3 (mixed isomers) and gypenoside XLIX showed a small increase in the ATP-induced YO-PRO-1 response which was not statistically significant (**Figure 2A**) whereas saikosaponin A and solanine both showed a large increase in the ATP-induced YO-PRO-1 dye uptake response (**Figure 2A**). Most other glycosides in this category showed no modulation of P2X7 (esculentoside A, mogroside V, glycyrrhizic acid, and stevioside). Stevenleaf showed a minor modulation increasing the maximum response only (1.64-fold; **Supplementary Figure 1**). Dose-response experiments demonstrated that gypenoside XVII has a Type II PAM activity at P2X7 (**Figure 2B**), reducing the EC_{50} value for ATP (Table 1) and increasing the maximum response 2-fold. In contrast, gypenoside XLIX did not reduce the EC_{50} value for ATP (Table 1) but did increase the maximum response by 1.9-fold (**Figure 2C**). Further investigations into saikosaponin A (**Figure 2D**) revealed that this glycoside increased YO-PRO-1 uptake at all concentrations of ATP tested and could induce YO-PRO-1 uptake in non-transfected HEK-293 cells (which have no expression of P2X7) and in HEK-hP2X7 cells in the absence of ATP (**Figure 2E**) suggesting that this effect was not P2X7-dependent. We confirmed this by pre-treating HEK-hP2X7 cells with a P2X7 selective antagonist, AZ10606120. ATP-induced responses were abolished in cells treated with 10 μM

Molecular Pharmacology Fast Forward. Published on December 17, 2020 as DOI: 10.1124/molpharm.120.000129
This article has not been copyedited and formatted. The final version may differ from this version.

AZ10606120 as were responses induced by ATP + CK (**Figure 2F**). However, responses to ATP + saikosaponin A or ATP + solanine were unaffected by AZ10606120 pre-treatment suggesting that P2X7 was not involved (**Figure 2F**).

We then investigated glycosides with monosaccharide attachments including daucosterol, ginsenoside-F2, ginsenoside-F1, ouabain and scilliroside (**Table 1**). Dose-response experiments demonstrated that ginsenoside-F2 could both increase the maximum response and reduce the EC_{50} value for ATP (**Table 1**) and displayed a similar mixed Type I/II effect as ginsenoside CK (**Figure 3D**). Ouabain, daucosterol and scilliroside had no effect on the ATP dose-response curves (**Figure 3**). Interestingly, ginsenoside-F1, which has an almost identical structure to CK, did not potentiate P2X7 responses (**Figure 3C**). The presence of one additional hydroxyl group on C-6 is the only difference between ginsenoside-CK and ginsenoside-F1 and this could potentially interfere with correct positioning into the P2X7 binding pocket.

Computational docking

To investigate the predicted theoretical docking differences between ginsenoside-CK and ginsenoside-F1 we used computational docking to a homology model of human P2X7 (Bidula et al., 2019b). Replacing ginsenoside-CK (**Figure 4A**) in the open ATP-bound model of hP2X7 with ginsenoside-F1 resulted in an analogous predicted pose (**Figure 4B**) and this would orient the additional hydroxyl group on C-6 to be facing the hydrophobic side of the pocket close to L320 and F322. Since ginsenoside-F1 has no activity at P2X7, this purely theoretical pose is suggestive that steric hindrance and a repulsive effect would prevent F1 from interacting with the PAM site at P2X7. Furthermore, there would likely be an energy penalty due to poor solvation of the additional OH group within the hydrophobic pocket.

Concurrently we investigated chemicals thought to bind in an inverted mode such as ginsenoside-Rd (Bidula et al., 2019b). Ginsenosides with sugars attached to C-3 rather than

Molecular Pharmacology Fast Forward. Published on December 17, 2020 as DOI: 10.1124/molpharm.120.000129
This article has not been copyedited and formatted. The final version may differ from this version.

C-20 are predicted to insert sugars deep into the pocket and would have the C-20 side chain solvent-exposed. We have previously demonstrated that the monosaccharide ginsenoside-Rh2 is able to potentiate hP2X7 responses (Helliwell et al., 2015) and have predicted a binding model (Bidula et al., 2019b). Ginsenosides Rh2 and Rg3 are also predicted to bind in this inverted mode and both of these ginsenosides can exist as two diasteromers with regard to the C-20 side chain. The natural product form in *Panax ginseng* is believed to be the 20(*S)*-diastereomer (Qi et al., 2011, Yang et al., 2014) and this is thought to have higher bioactivity than the 20(*R)*-diastereomer (Wei et al., 2012). We investigated the individual pure diastereomers to determine if this had any bearing on PAM activity at P2X7 and found that only the 20(*S)*-diastereomers of Rg3 and Rh2 are active as PAMs at hP2X7 (**Figure 5**). This suggests that the stereospecific positioning of the –OH group on C-20 may be critical for mediating the potentiating effect. To investigate which part of P2X7 would be closest to C-20, we used computational induced-fit docking using Glide as previously reported (Bidula et al., 2019b). The most populated pose for 20(*S)*-Rg3 is presented in **Figure 6** and this places the C-20 hydroxyl group pointing away from the hydrophobic side of the pocket. In an analogous theoretical pose, 20(*R)*-Rg3 would have this C-20 hydroxyl group in close proximity to the hydrophobic face increasing steric hindrance and repulsive effects plus the desolvation penalty as mentioned above, preventing 20(*R)*-Rg3 and 20(*R)*-Rh2 from interacting with the binding pocket on P2X7.

Modulation of endogenous human P2X7 in immune cells

Finally, we verified our findings on the identified active vs inactive glycosides by using a human THP-1 monocytic cell line known to endogenously express P2X7 (**Figure 7**). Using fura-2AM loaded cells, we measured ATP-induced calcium responses (**Figure 7A**) and found that there was a rapid peak increase in calcium followed by a sustained elevation of calcium over 300 seconds of recording. Pre-treatment of THP-1 cells with commercially available P2X7 selective antagonists such as AZ11645373 or AZ10606120 did not

Molecular Pharmacology Fast Forward. Published on December 17, 2020 as DOI: 10.1124/molpharm.120.000129
This article has not been copyedited and formatted. The final version may differ from this version.

dramatically affect the response to 500 μM ATP (**Figure 7**) but co-application of ginsenoside-CK with 500 μM ATP increased the peak response and the sustained elevation in $[Ca^{2+}]_i$ (**Figure 7**). This increased response could be completely abolished in cells pre-treated with either AZ11645373 (10 μM) or AZ10606120 (10 μM) suggesting that the ginsenoside-CK potentiated response is solely mediated by P2X7 with no involvement of other purinergic receptors. Using the same protocol we investigated whether we could verify active and inactive glycosides as PAMs and confirmed that ginsenosides F2, Rd and 20(*S)*-Rg3 all potentiated the ATP-induced calcium response in THP-1 cells and this potentiation was abolished by pre-treatment with a P2X7-selective antagonist (**Figure 7C**).

We then determined if the identified active PAMs ginsenoside F2, 20(*S)*-Rg3 and gypenoside XVII could enhance P2X7-dependent cell death in the highly expressing HEK-hP2X7 model using ginsenoside-CK as a positive control. Both ginsenoside-F2 and 20*(S)*-Rg3 could reduce cell viability over 24 hours when applied in combination with ATP and this was prevented by pre-treatment with AZ10606120 (**Figure 7D**). However, neither gypenoside XVII nor 20(*R)*-Rg3 in combination with ATP affected cell viability (**Figure 7D**). In THP-1 cells, treatment with 500 μM ATP significantly reduced cell viability to 73.3 ± 14.4 % of control (**Figure 7E**) although this may not be P2X7-dependent due to the lack of effect of AZ10606120. Only ginsenoside-CK could significantly enhance this ATP-induced cell death in THP-1 cells (**Figure 7E**).

Molecular Pharmacology Fast Forward. Published on December 17, 2020 as DOI: 10.1124/molpharm.120.000129
This article has not been copyedited and formatted. The final version may differ from this version.

Discussion

In summary, we have demonstrated that the chemical requirements for positive allosteric modulators at P2X7 appear to be quite stringent. Dose-response experiments demonstrate that ginsenoside-CK and ginsenoside-Rd have two effects on ATP-induced responses at hP2X7 (**Figure 1B**); an increase in the maximum response (a Type I PAM effect) and a shift in the dose-response curve to the left (a Type II PAM effect) thereby enhancing the maximum effect of the agonist and reducing the EC_{50} value. Our previous work has shown ginsenoside-CK, a triterpenoid glycoside with one glucose attachment, to have the best PAM effect at human P2X7. Here we show that ginsenoside-F2 and ginsenoside 20(*S)*-Rg3 have equivalent PAM activity at P2X7. We investigated a range of glycosides with different numbers of carbohydrate groups attached, and alternative sugar groups to glucose. Of these, gypenoside XVII showed the best PAM activity at P2X7. This glycoside is a dammarene glycoside found in *Panax* species, typically *Panax notoginseng* (Sakah et al., 2013). Gypenoside XVII has a single glucose attached at C-3 and two glucose groups attached at C-20 (a β-D-glucopyranosyl-(1-6)-β-D-glucopyranoside). It is very similar in structure to stevenleaf, (also known as gypenoside IX, **Table 1**) but the sugar attachments on C-20 are different. Stevenleaf has a glucose-xylose disaccharide attached at C-20 whereas in gypenoside XVII, this is a glucose-glucose disaccharide. The reduced activity of stevenleaf (**Supplementary Figure 1**) compared to gypenoside XVII suggests that there is a preferential requirement for glucose within the binding pocket on P2X7. Similarly esculentoside A has a similar structure to ginsenoside 20(*S)*-Rg3 with a disaccharide on C-3 although this is composed of glucose-xylose whereas Rg3 has a glucose-glucose disaccharide. Esculentoside A was inactive at P2X7 (**Supplementary Figure 1**).

Most useful in terms of defining a structure-activity relationship for PAMs at P2X7, was the finding that modifications at C-6 were not tolerated. Ginsenoside-F1 showed no PAM activity at P2X7 and computational docking suggests that this additional hydroxyl on C-6 faces the

Molecular Pharmacology Fast Forward. Published on December 17, 2020 as DOI: 10.1124/molpharm.120.000129
This article has not been copyedited and formatted. The final version may differ from this version.

hydrophobic side of the predicted binding pocket. This may be incompatible with binding to P2X7 in order to produce effective potentiation of responses. We have not performed a binding assay to determine if this lack of activity equates to a lack of binding to P2X7 rather than equivalent binding and a lack of effect. Currently there are no suitably labelled ginsenosides available as probes and this is something we shall explore in future studies. We also discovered that the stereochemistry of 20(*S)* vs 20(*R)* in the ginsenosides Rg3 and Rh2 have a clear effect on PAM activity with only the 20(*S)* diastereomers retaining good PAM activity. Again, computational docking suggests this C-20 hydroxyl group to be close to the highly hydrophobic side of the predicted binding pocket and we hypothesize that this is important in correct positioning leading to effective potentiation of ATP-dependent responses. Regarding the differences in the terpenoid backbone, several of the compounds we selected for testing contained carbohydrate at either end of the molecule but did not contain the dammarene scaffold. For example, daucosterol is a monosaccharide (glucose) but contains a sitosterol-like scaffold. This includes a double bond which changes the shape of the scaffold and has a detrimental effect on activity at P2X7. The key elements to the structure-activity relationship for glycosides at P2X7 are summarised in **Figure 8** showing two predicted binding modes for glycosides. Figure 8A shows the CK binding mode with C-20 glucose inserted into the binding pocket. Figure 8B shows the inverted mode for ginsenosides with C-3 glucose inserted into the binding pocket. Substitutions are tolerated on C-3 and C-20, but glucose is the preferred sugar attachment. Monosaccharides have higher activity than most disaccharides, and no substitution is tolerated at C-6 (**Figure 8A**). In the inverted mode, the stereochemistry of the hydroxyl on C-20 is critical for activity (**Figure 8B**). In both cases the dammarene scaffold is favoured over a sitosterol scaffold.

It is important to perform full dose-response analysis to determine those compounds that have PAM effects at P2X7. Saikosaponin A and solanine could increase the ATP-induced dye uptake in the screen on HEK-hP2X7 cells (**Figure 2A**) but further investigation showed that these compounds had a toxic effect on the cells, inducing YO-PRO-1 dye

Molecular Pharmacology Fast Forward. Published on December 17, 2020 as DOI: 10.1124/molpharm.120.000129
This article has not been copyedited and formatted. The final version may differ from this version.

uptake in the absence of ATP or the absence of the P2X7 receptor (**Figure 2**). Saikosaponins have been linked to multiple biological effects including induction of apoptosis (Li et al., 2018).

Several groups have demonstrated endogenous steroidal compounds to have positive allosteric modulator activity at P2X receptors. Dehydroepiandrosterone and progesterone can potentiate rodent P2X2 receptors (De Roo et al., 2010, De Roo et al., 2003) and 17β-ester derivatives of testosterone also potentiate rat P2X2 and P2X4 (Sivcev et al., 2019). None of these compounds had activity at P2X7 receptors. Lithocholic acid, a bile acid, has potentiating activity at P2X7 and P2X4 (rat) but inhibits rat P2X2 (Sivcev et al., 2020). This suggests there may exist endogenous regulators of P2X channel activity. It has been suggested that the bile acids may share a similar binding site to ivermectin, close to TM1 (Sivcev et al., 2020).

Positive allosteric modulation of P2X7 may be important in a number of contexts (Stokes et al., 2020). In this study we used the human monocytic cell line, THP-1 which has been used in other studies to investigate human P2X7 responses (Gadeock et al., 2010, Stokes et al., 2006). Native P2X7 responses are small in this cell line, likely masked by the multitude of other purinergic ATP-responsive receptors present. P2X7-selective antagonists did not affect the ATP-induced calcium responses dramatically (**Figure 7A**) yet we did see robust potentiation of the ATP-induced calcium response which was mediated by P2X7. The THP-1 cell line carries a loss-of-function polymorphism in the C-terminus of P2X7, rs3751143 encoding the Glu496>Ala substitution. Sequencing of exon 13 reveals heterozygosity for rs3751143 (**Supplementary Figure 2**) confirming the work in (Gadeock et al., 2012). Therefore, our data clearly shows that P2X7 responses in THP-1 cells can be enhanced by CK and we can effectively rescue deficient P2X7 receptor responses in humans carrying this loss-of-function polymorphism. Ginsenosides F2 and Rd were also effective at increasing P2X7 responses in THP-1 cells (**Figure 7**) and ginsenoside-F1 was inactive. Extending this set of data which measures immediate P2X7 responses, we looked

Molecular Pharmacology Fast Forward. Published on December 17, 2020 as DOI: 10.1124/molpharm.120.000129
This article has not been copyedited and formatted. The final version may differ from this version.

at P2X7-mediated cell death first in HEK-hP2X7 cells using an Alamar Blue viability assay. Ginsenosides CK, Rd, 20(*S*)-Rg3 and F2 were very effective at enhancing cell death in combination with ATP, however, gypenoside XVII was unable to enhance P2X7-mediated cell death in this cell line (**Figure 7D**). At this stage, it is unclear why this would be the case. Future investigations into the longevity of the potentiation may reveal that gypenoside XVII has a shorter duration of action than the ginsenosides perhaps due to differential binding modes. Repeating this work in THP-1 cells showed that only ginsenoside-CK was effective at potentiation of cell death induced by ATP (**Figure 7E**). This may be due to the lower level of expression of P2X7 in THP-1 cells, the expression of other purinergic receptors that may bind ginsenosides such as P2X4, or simply due to duration of action. It is also conceivable that monocytes may release factors such as glycosidase enzymes that can degrade ginsenosides.

Other compounds can act as positive allosteric modulators of P2X7 (Stokes et al., 2020) including clemastine (Norenberg et al., 2011), tenidap (Sanz et al., 1998), ivermectin (Nörenberg et al., 2012) and polymyxin B (Ferrari et al., 2004). These bear no structural similarities to ginsenosides although ivermectin is a glycoside, containing two oleandrose sugars. As yet nothing is known about the potential site of action of ivermectin on P2X7 although on P2X4 the site is proposed to be close to TM1 (Asatryan et al., 2010, Samways et al., 2012). In terms of therapeutic relevance of PAMs acting at P2X7, most exciting is the potential to enhance the microbicidal activity of immune cells. P2X7 has been implicated in regulation of pathogen killing, particularly those which reside in intracellular locations such as mycobacteria and parasites (Di Virgilio et al., 2017, Savio et al., 2018). The mechanisms by which P2X7 contributes to reduction of pathogen burden are not yet well understood but could involve cytokine/mediator secretion, ROS generation or host cell apoptosis. Potentiation of P2X7 responses with ginsenoside-CK changed the type of cell death in J774 macrophage cell line compared to high concentrations of ATP (Bidula et al., 2019a) and this could be relevant within an immune response. In models of infection, most of the work has

Molecular Pharmacology Fast Forward. Published on December 17, 2020 as DOI: 10.1124/molpharm.120.000129
This article has not been copyedited and formatted. The final version may differ from this version.

been performed on P2X7 deficient mice to understand the role of this receptor within the host immune response. However, there has not been an *in vivo* study to investigate pharmacological targeting of P2X7 with a PAM. This idea has been tested in a zebrafish whole-animal study for *Mycobacterium marinum* infection using clemastine to potentiate P2X7 (Matty et al., 2019) providing evidence that targeting P2X7 may be beneficial to control mycobacterial infections.

Molecular Pharmacology Fast Forward. Published on December 17, 2020 as DOI: 10.1124/molpharm.120.000129
This article has not been copyedited and formatted. The final version may differ from this version.

Acknowledgements:

Author contributions:

Participated in research design: Stokes, Ganesan, Bidula

Conducted experiments: Piyasirananda, Stokes, Beekman

Performed data analysis: Piyasirananda, Stokes, Beekman

Wrote, or contributed to writing of the manuscript: Piyasirananda, Stokes, Beekman, Ganesan, Bidula.

Molecular Pharmacology Fast Forward. Published on December 17, 2020 as DOI: 10.1124/molpharm.120.000129
This article has not been copyedited and formatted. The final version may differ from this version.

References

AREESHI, M. Y., MANDAL, R. K., DAR, S., WAHID, M., KHAN, M. E., PANDA, A. K., JAWED, A. & HAQUE, S. 2015. P2X71513 A>C Polymorphism Confers Increased Risk of Extrapulmonary Tuberculosis: A Meta-analysis of Case-Control Studies. *Curr Genomics,* 17**,** 450-458.

ASATRYAN, L., POPOVA, M., PERKINS, D., TRUDELL, J. R., ALKANA, R. L. & DAVIES, D. L. 2010. Ivermectin antagonizes ethanol inhibition in purinergic P2X4 receptors. *J Pharmacol Exp Ther,* 334**,** 720-8.

BIDULA, S., DHUNA, K., HELLIWELL, R. & STOKES, L. 2019a. Positive allosteric modulation of P2X7 promotes apoptotic cell death over lytic cell death responses in macrophages. *Cell Death Dis,* 10**,** 882.

BIDULA, S. M., CROMER, B. A., WALPOLE, S., ANGULO, J. & STOKES, L. 2019b. Mapping a novel positive allosteric modulator binding site in the central vestibule region of human P2X7. *Sci Rep,* 9**,** 3231.

CHAVES, M. M., MARQUES-DA-SILVA, C., MONTEIRO, A. P., CANETTI, C. & COUTINHO-SILVA, R. 2014. Leukotriene B4 modulates P2X7 receptor-mediated Leishmania amazonensis elimination in murine macrophages. *J Immunol,* 192**,** 4765-73.

CHAVES, M. M., SINFLORIO, D. A., THORSTENBERG, M. L., MARTINS, M. D. A., MOREIRA-SOUZA, A. C. A., RANGEL, T. P., SILVA, C. L. M., BELLIO, M., CANETTI, C. & COUTINHO-SILVA, R. 2019. Non-canonical NLRP3 inflammasome activation and IL-1β signaling are necessary to L. amazonensis control mediated by P2X7 receptor and leukotriene B4. *PLoS pathogens,* 15**,** e1007887-e1007887.

DE ROO, M., BOUÉ-GRABOT, E. & SCHLICHTER, R. 2010. Selective potentiation of homomeric P2X2 ionotropic ATP receptors by a fast non-genomic action of progesterone. *Neuropharmacology,* 58**,** 569-577.

DE ROO, M., RODEAU, J. L. & SCHLICHTER, R. 2003. Dehydroepiandrosterone potentiates native ionotropic ATP receptors containing the P2X2 subunit in rat sensory neurones. *J Physiol,* 552**,** 59-71.

DI VIRGILIO, F., DAL BEN, D., SARTI, A. C., GIULIANI, A. L. & FALZONI, S. 2017. The P2X7 Receptor in Infection and Inflammation. *Immunity,* 47**,** 15-31.

FAIRBAIRN, I. P., STOBER, C. B., KUMARARATNE, D. S. & LAMMAS, D. A. 2001. ATP-mediated killing of intracellular mycobacteria by macrophages is a P2X(7)-dependent process inducing bacterial death by phagosome-lysosome fusion. *Journal of immunology (Baltimore, Md. : 1950),* 167**,** 3300-3307.

FERNANDO, S. L., SAUNDERS, B. M., SLUYTER, R., SKARRATT, K. K., GOLDBERG, H., MARKS, G. B., WILEY, J. S. & BRITTON, W. J. 2007. A polymorphism in the P2X7 gene increases susceptibility to extrapulmonary tuberculosis. *Am J Respir Crit Care Med,* 175**,** 360-6.

FERRARI, D., PIZZIRANI, C., ADINOLFI, E., FORCHAP, S., SITTA, B., TURCHET, L., FALZONI, S., MINELLI, M., BARICORDI, R. & DI VIRGILIO, F. 2004. The antibiotic polymyxin B modulates P2X7 receptor function. *J Immunol,* 173**,** 4652-60.

FRIESNER, R. A., BANKS, J. L., MURPHY, R. B., HALGREN, T. A., KLICIC, J. J., MAINZ, D. T., REPASKY, M. P., KNOLL, E. H., SHELLEY, M., PERRY, J. K., SHAW, D. E., FRANCIS, P. & SHENKIN, P. S. 2004. Glide: a new approach for rapid, accurate docking and scoring. 1. Method and assessment of docking accuracy. *J Med Chem,* 47**,** 1739-49.

GADEOCK, S., J, T., GEORGIOU, J. G., JALILIAN, I., TAYLOR, R. M., WILEY, J. S. & SLUYTER, R. 2010. TGF-β1 prevents up-regulation of the P2X7 receptor by IFN-γ and LPS in leukemic THP-1 monocytes. *Biochim. Biophys. Acta,* 1798**,** 2058-2066.

GADEOCK, S., PUPOVAC, A., SLUYTER, V., SPILDREJORDE, M. & SLUYTER, R. 2012. P2X7 receptor activation mediates organic cation uptake into human myeloid leukaemic KG-1 cells. *Purinergic Signal,* 8**,** 669-76.

GIULIANI, A. L., SARTI, A. C., FALZONI, S. & DI VIRGILIO, F. 2017. The P2X7 Receptor-Interleukin-1 Liaison. *Frontiers in Pharmacology,* 8**,** 123.

HACKOS, D. H. & HANSON, J. E. 2017. Diverse modes of NMDA receptor positive allosteric modulation: Mechanisms and consequences. *Neuropharmacology,* 112**,** 34-45.

HALGREN, T. 2007. New method for fast and accurate binding-site identification and analysis. *Chem Biol Drug Des,* 69**,** 146-8.

HELLIWELL, R. M., SHIOUKHUEY, C. O., DHUNA, K., MOLERO, J. C., YE, J. M., XUE, C. C. & STOKES, L. 2015. Selected ginsenosides of the protopanaxdiol series are novel positive allosteric modulators of P2X7 receptors. *Br J Pharmacol,* 172**,** 3326-40.

JACOBSON, M. P., PINCUS, D. L., RAPP, C. S., DAY, T. J., HONIG, B., SHAW, D. E. & FRIESNER, R. A. 2004. A hierarchical approach to all-atom protein loop prediction. *Proteins,* 55**,** 351-67.

LI, X., LI, X., HUANG, N., LIU, R. & SUN, R. 2018. A comprehensive review and perspectives on pharmacology and toxicology of saikosaponins. *Phytomedicine,* 50**,** 73-87.

MATTY, M. A., KNUDSEN, D. R., WALTON, E. M., BEERMAN, R. W., CRONAN, M. R., PYLE, C. J., HERNANDEZ, R. E. & TOBIN, D. M. 2019. Potentiation of P2RX7 as a host-directed strategy for control of mycobacterial infection. *eLife,* 8**,** e39123.

MILLER, C. M., ZAKRZEWSKI, A. M., ROBINSON, D. P., FULLER, S. J., WALKER, R. A., IKIN, R. J., BAO, S. J., GRIGG, M. E., WILEY, J. S. & SMITH, N. C. 2015. Lack of a Functioning P2X7 Receptor Leads to Increased Susceptibility to Toxoplasmic Ileitis. *PLoS One,* 10**,** e0129048.

MOREIRA-SOUZA, A. C. A., ALMEIDA-DA-SILVA, C. L. C., RANGEL, T. P., ROCHA, G. D. C., BELLIO, M., ZAMBONI, D. S., VOMMARO, R. C. & COUTINHO-SILVA, R. 2017. The P2X7 Receptor Mediates Toxoplasma gondii Control in Macrophages through Canonical NLRP3 Inflammasome Activation and Reactive Oxygen Species Production. *Front Immunol,* 8**,** 1257.

NORENBERG, W., HEMPEL, C., URBAN, N., SOBOTTKA, H., ILLES, P. & SCHAEFER, M. 2011. Clemastine potentiates the human P2X7 receptor by sensitizing it to lower ATP concentrations. *J Biol Chem,* 286**,** 11067-81.

NÖRENBERG, W., SOBOTTKA, H., HEMPEL, C., PLÖTZ, T., FISCHER, W., SCHMALZING, G. & SCHAEFER, M. 2012. Positive allosteric modulation by ivermectin of human but not murine P2X7 receptors. *British Journal of Pharmacology,* 167**,** 48-66.

PLACIDO, R., AURICCHIO, G., FALZONI, S., BATTISTINI, L., COLIZZI, V., BRUNETTI, E., DI VIRGILIO, F. & MANCINO, G. 2006. P2X(7) purinergic receptors and extracellular ATP mediate apoptosis of human monocytes/macrophages infected with Mycobacterium tuberculosis reducing the intracellular bacterial viability. *Cellular immunology,* 244**,** 10-18.

QI, L. W., WANG, C. Z. & YUAN, C. S. 2011. Ginsenosides from American ginseng: chemical and pharmacological diversity. *Phytochemistry,* 72**,** 689-99.

SAKAH, K. J., WANG, T., LIU, L., CHEN, Y., HAN, L. & ZHANG, Y. 2013. Eight darmarane-type saponins isolated from the roots of Panax notoginseng. *Acta Pharmaceutica Sinica B,* 3**,** 381-384.

SAMWAYS, D. S., KHAKH, B. S. & EGAN, T. M. 2012. Allosteric modulation of Ca2+ flux in ligand-gated cation channel (P2X4) by actions on lateral portals. *J Biol Chem,* 287**,** 7594-602.

SANZ, J. M., CHIOZZI, P. & DI VIRGILIO, F. 1998. Tenidap enhances P2Z/P2X7 receptor signalling in macrophages. *Eur J Pharmacol,* 355**,** 235-44.

SAVIO, L. E. B., DE ANDRADE MELLO, P., DA SILVA, C. G. & COUTINHO-SILVA, R. 2018. The P2X7 Receptor in Inflammatory Diseases: Angel or Demon? *Front Pharmacol,* 9**,** 52.

SIVCEV, S., SLAVIKOVA, B., IVETIC, M., KNEZU, M., KUDOVA, E. & ZEMKOVA, H. 2020. Lithocholic acid inhibits P2X2 and potentiates P2X4 receptor channel gating. *The Journal of Steroid Biochemistry and Molecular Biology***,** 105725.

SIVCEV, S., SLAVIKOVA, B., RUPERT, M., IVETIC, M., NEKARDOVA, M., KUDOVA, E. & ZEMKOVA, H. 2019. Synthetic testosterone derivatives modulate rat P2X2 and P2X4 receptor channel gating. *Journal of Neurochemistry,* 150**,** 28-43.

STOKES, L., BIDULA, S., BIBIC, L. & ALLUM, E. 2020. To inhibit or enhance? Is there a benefit to positive allosteric modulation of P2X receptors? . *Frontiers in Pharmacology,* 11.

STOKES, L., JIANG, L. H., ALCARAZ, L., BENT, J., BOWERS, K., FAGURA, M., FURBER, M., MORTIMORE, M., LAWSON, M., THEAKER, J., LAURENT, C., BRADDOCK, M. & SURPRENANT, A. 2006. Characterization of a selective and potent antagonist of human P2X(7) receptors, AZ11645373. *Br J Pharmacol,* 149**,** 880-7.

WEI, X., CHEN, J., SU, F., SU, X., HU, T. & HU, S. 2012. Stereospecificity of ginsenoside Rg3 in promotion of the immune response to ovalbumin in mice. *Int Immunol,* 24**,** 465-71.

YANG, W. Z., HU, Y., WU, W. Y., YE, M. & GUO, D. A. 2014. Saponins in the genus Panax L. (Araliaceae): a systematic review of their chemical diversity. *Phytochemistry,* 106**,** 7-24.

Molecular Pharmacology Fast Forward. Published on December 17, 2020 as DOI: 10.1124/molpharm.120.000129
This article has not been copyedited and formatted. The final version may differ from this version.

Footnotes:

This work was supported by a Royal Thai government funded PhD scholarship to WP and a BBSRC project grant to LS (BB/N018427/1).

Molecular Pharmacology Fast Forward. Published on December 17, 2020 as DOI: 10.1124/molpharm.120.000129
This article has not been copyedited and formatted. The final version may differ from this version.

Figure Legends

Figure 1: Positive allosteric effect of protopanaxadiol ginsenosides on P2X7.

(**A**) A YO-PRO-1 iodide uptake assay was used to determine the effect of multiple ginsenosides on human P2X7 stably expressed in HEK-293 cells. Agonist (ATP, 200 μM) and modulator (10 μM) were pre-mixed at 10X final concentration and auto-injected together (co-injection) using a Flexstation 3 multimode plate reader. YO-PRO-1 dye uptake was measured over 300 seconds. Data is mean +/- standard deviation (**B**) Dose-response curves to ATP in the absence and presence of 10 μM ginsenoside CK, Rd, Rb1, or the aglycone PPD with a four-parameter non-linear regression. Data is collated from 3 independent experiments each performed in triplicate. Error bars represent standard deviation. **(C)** Chemical structures for each of the ginsenoside positive modulators and the inactive aglycone PPD are shown.

Figure 2: Screening glycosides containing disaccharide and trisaccharide moieties at P2X7. (**A**) Initial experiments used a fixed concentration of ATP (200 μM final) and glycoside (10 μM final) to screen selected glycosides at P2X7. Data is collated from 2-4 independent experiments. Ginsenoside CK was used as the control PAM and is shown in blue. YO-PRO-1 uptake was measured as area under curve (50-300 seconds) and data is expressed as percentage of control where the control is ATP + DMSO. One-way ANOVA with Dunnett's multiple comparisons test was performed and * represents $P<0.05$ compared to DMSO control. (**B**) Dose-response curve to ATP in the presence of vehicle (DMSO), ginsenoside CK or gypenoside XVII (10 μM). (**C**) Dose-response curve to ATP in the presence of vehicle (DMSO), ginsenoside CK or gypenoside XLIX (10 μM). (**D**) Dose-response curve to ATP in the presence of vehicle (DMSO), ginsenoside CK or saikosaponin A (10 μM). Data points are mean +/- standard deviation. The same curves from DMSO and ginsenoside CK are shown in panels B-D (**E**) Summary of data from YO-PRO-1 uptake experiments in HEK-hP2X7 cells or parental non-transfected HEK-293 cells in response to drug alone (saikosaponin A or solanine) (**F**) Lack of effect of the P2X7-selective antagonist AZ10606120 (10 μM) on ATP-induced YO-PRO-1 uptake when solanine or saikosaponin were used. One-way ANOVA with Sidak's multiple comparisons test was performed and * represents $P<0.05$.

Figure 3: Screening glycosides containing monosaccharide moieties at P2X7. Dose-response curves to ATP in the presence of vehicle (DMSO), ginsenoside CK or (**A**) daucosterol (10 μM), (**B**) Stevioside (10 μM), (**C**) ginsenoside F1 (10 μM), (**D**) ginsenoside F2 (10 μM), (**E**) ouabain (10 μM), or (**F**) scilliroside (10 μM). Ginsenoside CK is demonstrated throughout as the reference compound (same data shown in each plot). Data is collated from 3 independent experiments each performed in triplicate. Error bars represent standard deviation.

Figure 4: Molecular docking of ginsenoside-CK and ginsenoside-F1 to the central vestibule pocket of hP2X7. Ginsenoside-CK (cyan) docked into the central vestibule in the ATP-bound homology model of human P2X7 and right, ginsenoside-F1 (green) docked into the same site. Side chains of residues of hP2X7 implicated in interactions are shown.

Molecular Pharmacology Fast Forward. Published on December 17, 2020 as DOI: 10.1124/molpharm.120.000129
This article has not been copyedited and formatted. The final version may differ from this version.

Figure 5: Diastereoisomers of ginsenosides have different activity at hP2X7.

(**A**) Dose-response curves to ATP in the presence of vehicle (DMSO), 20(*S)*-ginsenoside Rg3 or 20(*R)*-ginsenoside Rg3 (10 µM), (**B**) ginsenoside 20*(S)*-Rh2 or 20*(R)*-Rh2 (10 µM). Data is collated from 3 independent experiments and is mean +/- standard deviation. The same DMSO data is shown in both plots. Chemical structures of ginsenosides Rg3 and Rh2 are shown with the stereo-centres highlighted in red.

Figure 6: Induced-fit docking of 20S-Rg3 at human P2X7

Ginsenoside-20(*S)*-Rg3 (green) docked into the central vestibule site in a homology model of ATP-bound human P2X7 (open state). The predicted orientation of the stereocentre C-20 is such that the –OH is pointing away from the hydrophobic face of the binding site thus minimising any repulsive interactions. Key side chains of residues D318, L320 and F322 are indicated.

Figure 7: The PAM effects of glycosides in human THP-1 monocyte cell line.

(**A**) ATP-induced calcium responses were measured in fura-2AM loaded THP-1 cells in suspension using a Flexstation 3 plate reader. Agonist (500 µM ATP) and PAM (ginsenoside CK 10 µM) were co-injected following establishment of a baseline for 40 seconds. Cells were pre-incubated with various P2X7 antagonists for 10 minutes prior to start of plate recordings. (**B**) Summary of collated data from calcium measurements. Fura-2 responses were calculated as area under curve. Data was analysed using one-way ANOVA with Tukey's multiple comparisons test to assess the effect of antagonists. * represents P<0.05. (**C**) Investigating the P2X7 dependence of glycoside effects on ATP-induced calcium responses. AZ10606120 (10 µM) was added to cells to block P2X7 receptors prior to measuring calcium responses. Data was analysed using one-way ANOVA with Dunnett's multiple comparison test comparing each column against the control (500 µM ATP+DMSO). * represents P<0.05. (**D**) Cell viability experiments were performed over 24 hours using HEK-hP2X7 cell line. Alamar blue fluorescence was measured and data was normalised to % of control (DMSO). Data was collated from 5 independent experiments. One-way ANOVA was used to analyse the data with Sidak's multiple comparisons test to compare selected pairs of columns (DMSO+ATP vs ginsenoside+ATP). * represents P<0.05. **(E)** Cell viability experiments were performed over 24 hours using THP-1 cells. Alamar blue fluorescence was measured and data was normalised to % of control (DMSO). Data was collated from 5 independent experiments. One-way ANOVA was used to analyse the data with Sidak's multiple comparisons test to compare selected pairs of columns (DMSO+ATP vs ginsenoside+ATP). * represents P<0.05.

Figure 8: Proposed structure-activity relationship for glycosides acting as PAMs at P2X7. (A) The chemical structure of ginsenoside CK is shown with important groups highlighted. Glucose attachment (cyan) is critical for activity at P2X7. C-6 substitutions are not tolerated (yellow). (B) The chemical structure of ginsenoside 20*(S)*-Rg3 is demonstrated with positioning relative to the P2X7 binding mode (inverted). The C-3 glucose attachments (cyan) face up into the binding pocket. The C-20 hydroxyl group shows stereochemistry and positioning is critical for activity at P2X7.

Molecular Pharmacology Fast Forward. Published on December 17, 2020 as DOI: 10.1124/molpharm.120.000129
This article has not been copyedited and formatted. The final version may differ from this version.

Molecular Pharmacology Fast Forward. Published on December 17, 2020 as DOI: 10.1124/molpharm.120.000129
This article has not been copyedited and formatted. The final version may differ from this version.

Tables:

Table 1: Structural details of tested glycosides.

*Substitution pattern is derived from Figure 1C. Maximum response was defined at 1mM ATP. N.A. denotes not applicable. N.d = not determined. To calculate the EC_{50} ratio the average EC_{50} value for ATP + vehicle was used from each set of experiments. Average EC_{50} value is shown ± standard deviation. * represents P<0.05 from one-way ANOVA with Dunnett's multiple comparisons test.*

Glycoside	**ATP EC_{50} (**μM)	**EC_{50} Ratio**	**Maximum response** *(fold increase)*	**Substitution pattern**		
				R1 (C3)	**R2 (C6)**	**R3 (C20)**
Ginsenoside CK	61.6 ± 14.9 *	2.7	2.4-4.4	-OH		-glc
Ginsenoside F1	182.3 ± 36.7	1.1	1.46	-OH	-OH	-glc
Ginsenoside F2	35.3 ± 19.2 *	5.4	2.23	-glc		-glc
Ginsenoside 20(*S*)-Rh2	80.0 ± 20.9 *	1.8	2.6	-glc		-OH
Ginsenoside 20(*R*)-Rh2	169.7 ± 47.7	0.8	1.53	-glc		-OH
Daucosterol	258.5 ± 81.9	0.7	1.33	-glc		
Ouabain	133.4 ± 24.6	1.1	1.08	-rha		butyrolactone
Scilliroside	112.6 ± 27.8	1.3	1.07	-glc	-OAc	2-pyrone
Stevenleaf (gypenoside IX)	184.2 ± 45.5	0.7	1.64	-glc		-glc-xyl
Gypenoside XVII	79.9 ± 15.0 *	2.4	2.0	-glc		-glc-glc
Esculentoside A	165.5 ± 32.3	0.8	0.94	-xyl-glc		-COOMe
Ginsenoside 20(*S*)-Rg3	78.7 ± 23.9 *	1.8	2.4	-glc-glc		-OH
Ginsenoside 20(*R*)-Rg3	146 ± 24.1	1.0	0.94	-glc-glc		-OH
Ginsenoside Rd	57.7 ± 9.6 *	3.8	2.77	-glc-glc		-glc
Ginsenoside Rb1	175.9 ± 96.8	1.2	1.96	-glc-glc		-glc-glc
Stevioside	189.6 ± 39.0	1.0		-glc		-glc-glc
Glycyrrhizic acid	n.d	n.d	n.d	-glcA-glcA		-COOH
Saikosaponin A	N.A	n.d	N.A	-fuc-glc		
Gypenoside XLIX	213.1 ± 0.4	0.9	1.9	-rha-ara-xyl		-glc
Mogroside V	n.d	n.d	n.d	-glc-glc		-glc-glc-glc
Solasonine	N.A	n.d	N.A	-rha-gal-glc		
Solanine	N.A	n.d	N.A	-rha-gal-glc		

Figure 1

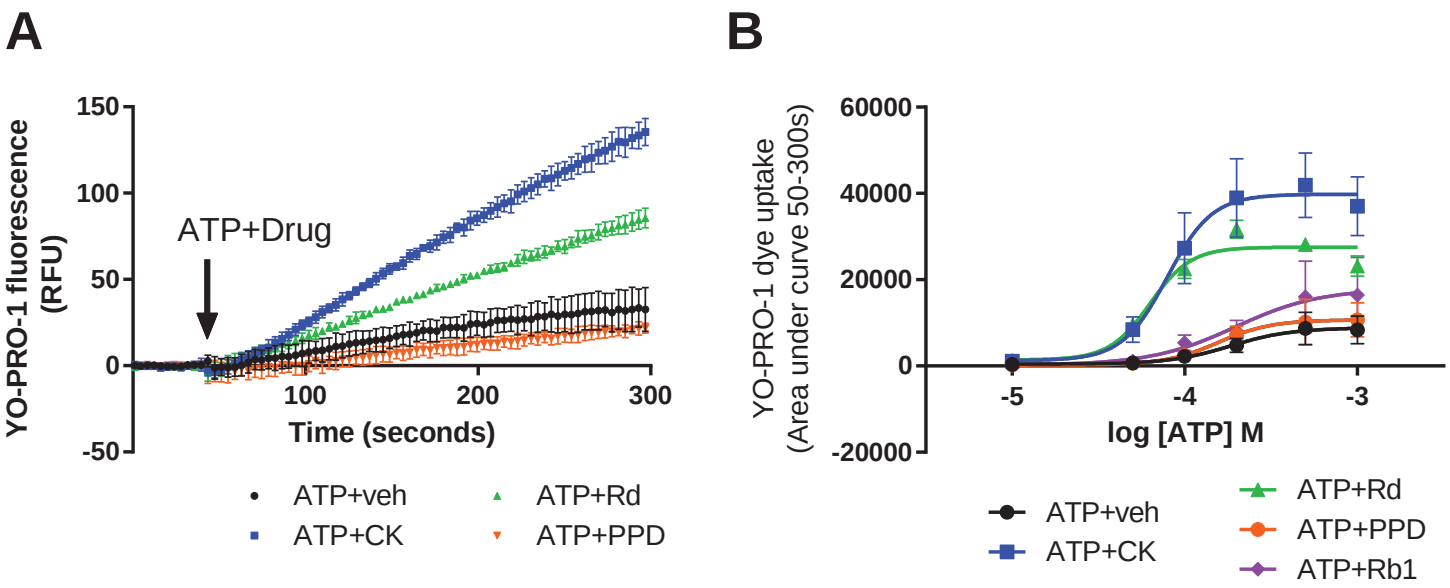

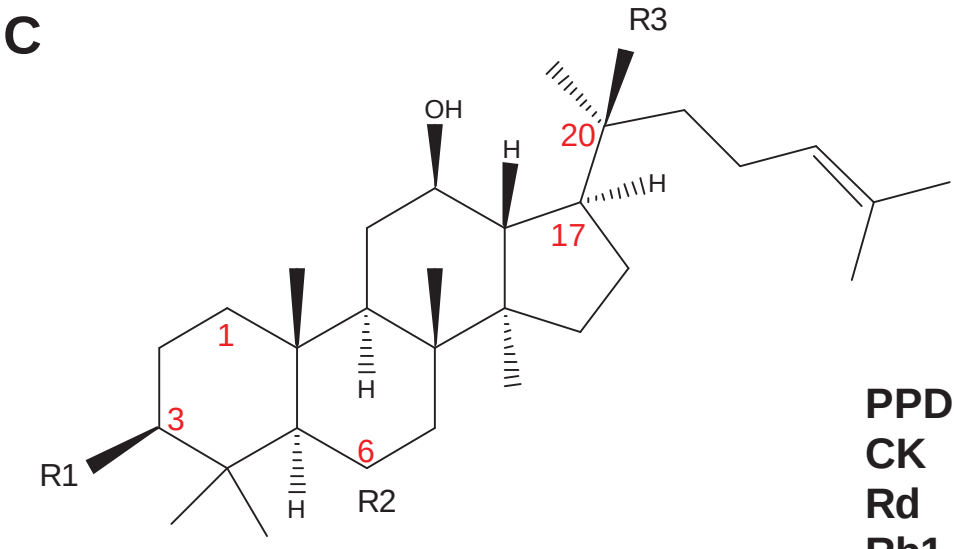

	R1	R2	R3
PPD	-OH	-H	-OH
CK	-OH	-H	-glc
Rd	-glcglc	-H	-glc
Rb1	-glcglc	-H	-glcglc

Figure 2

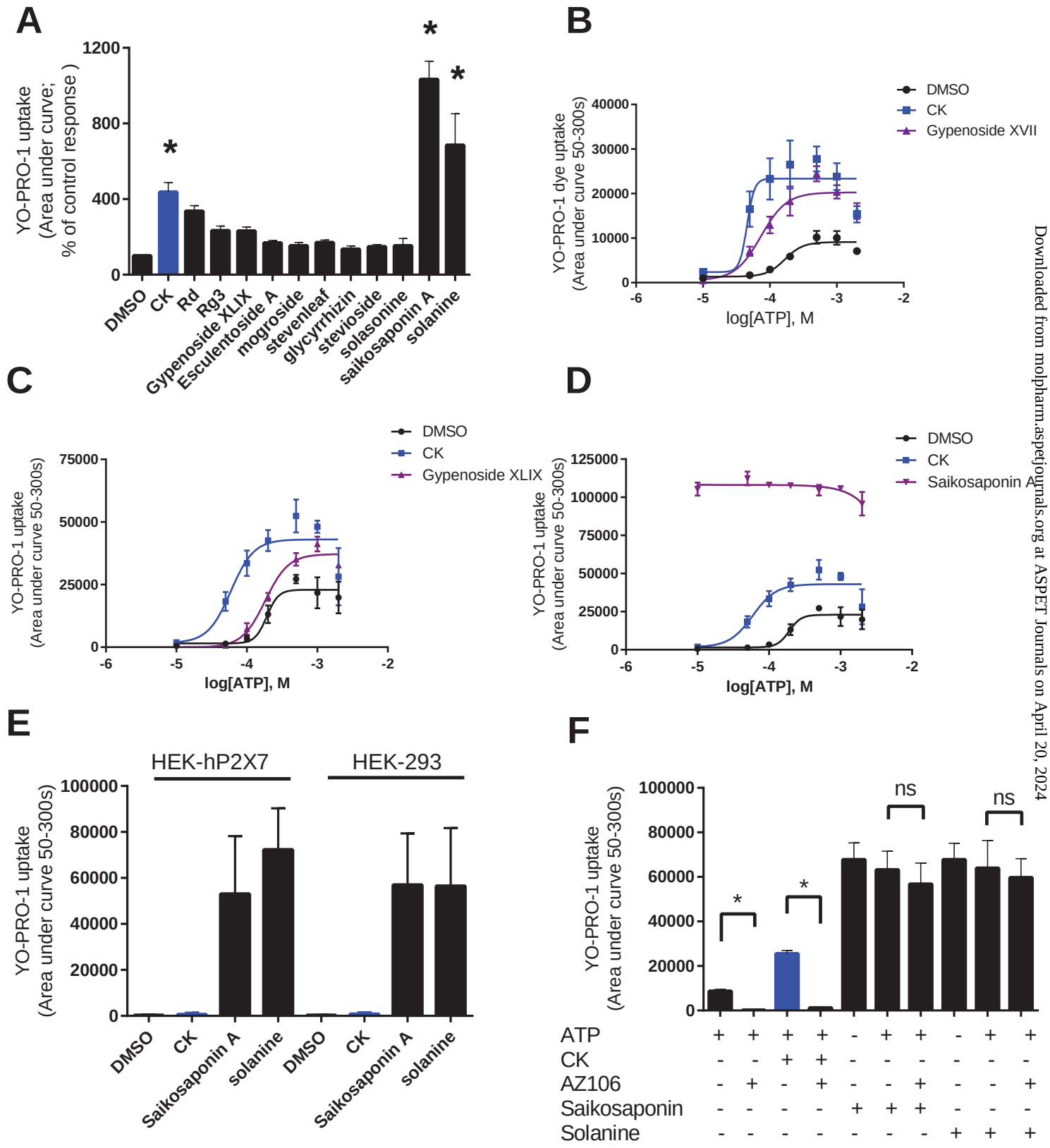

Figure 3

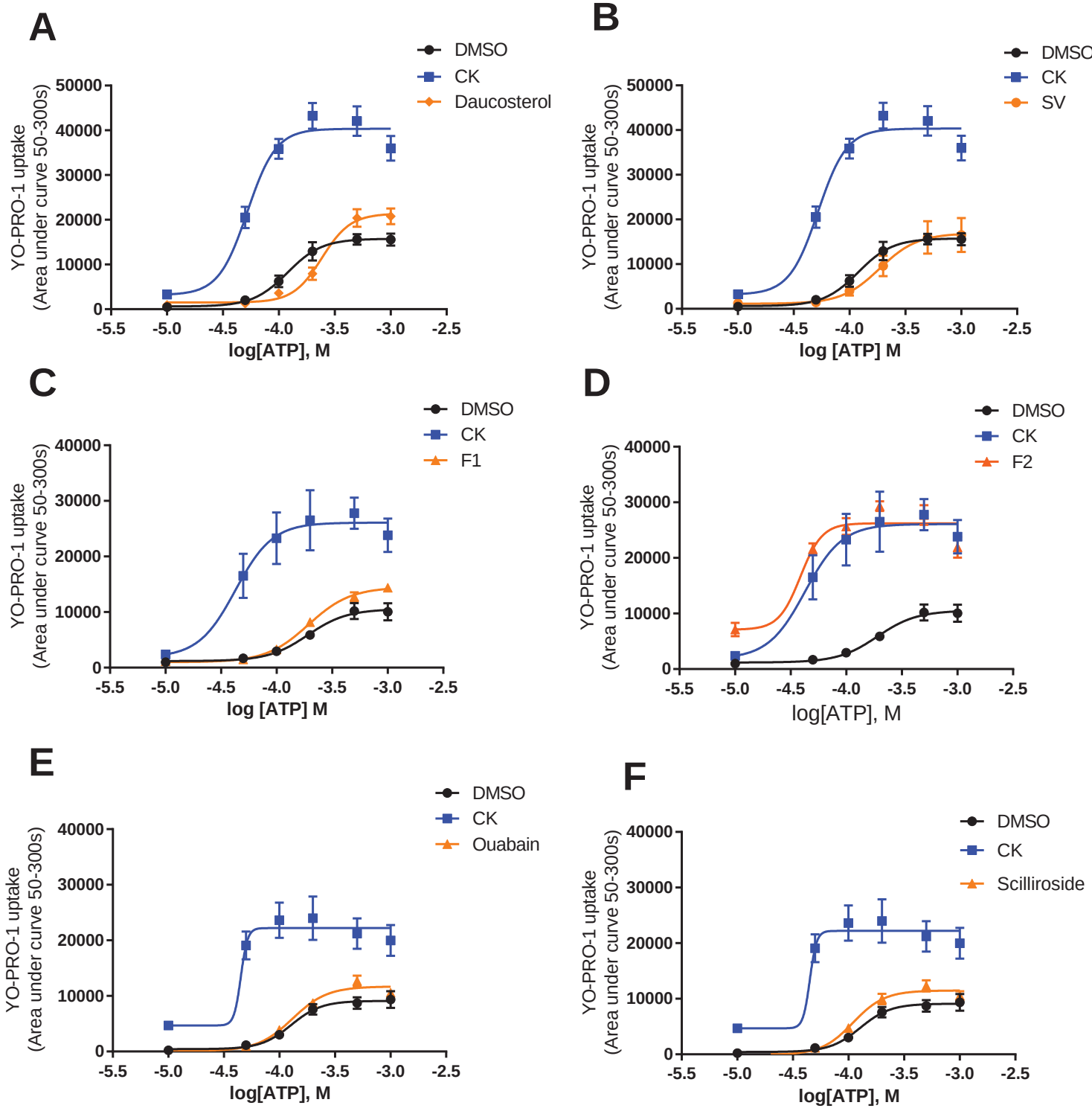

Figure 4

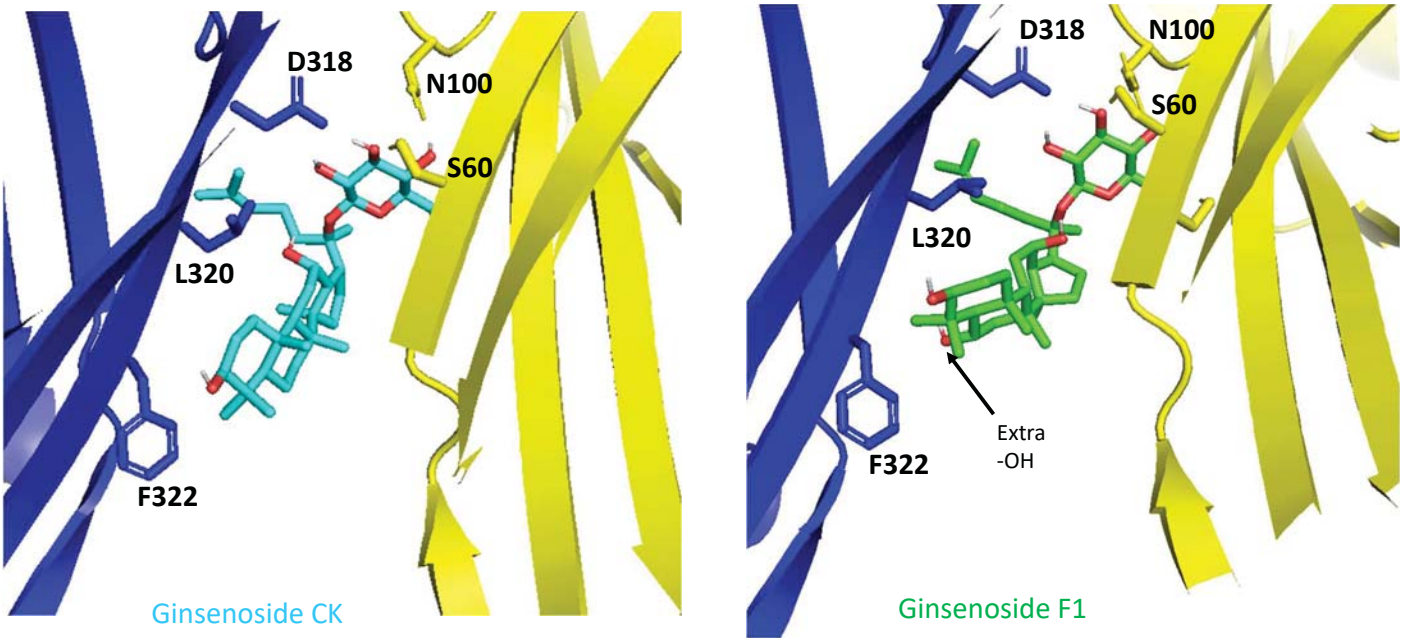

Figure 5

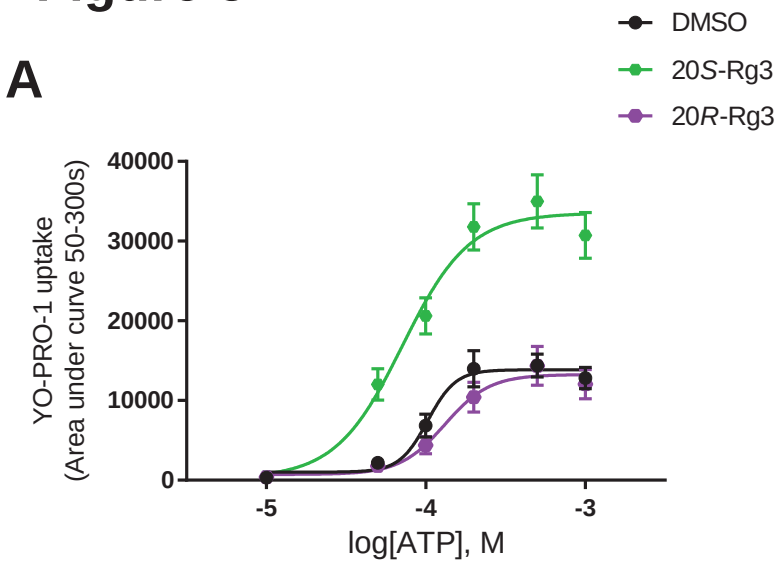

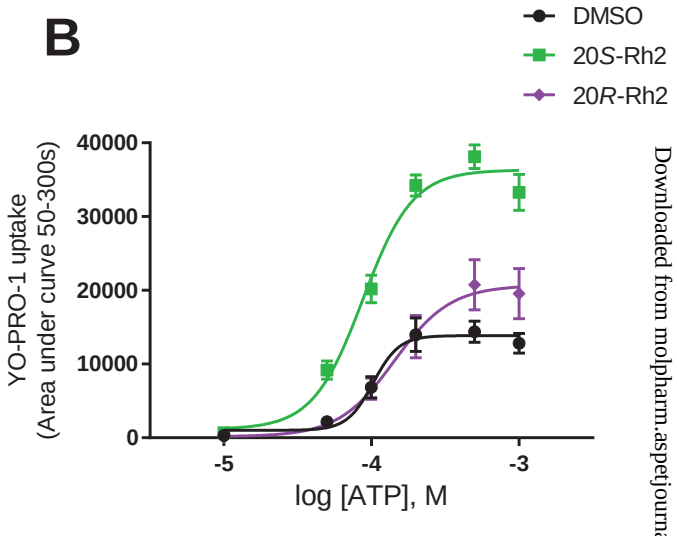

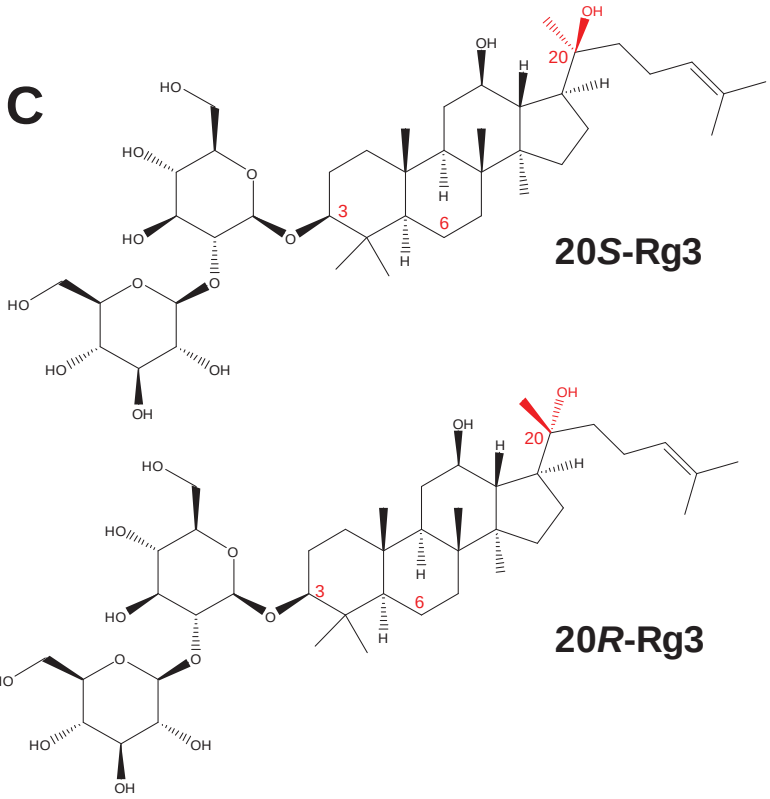

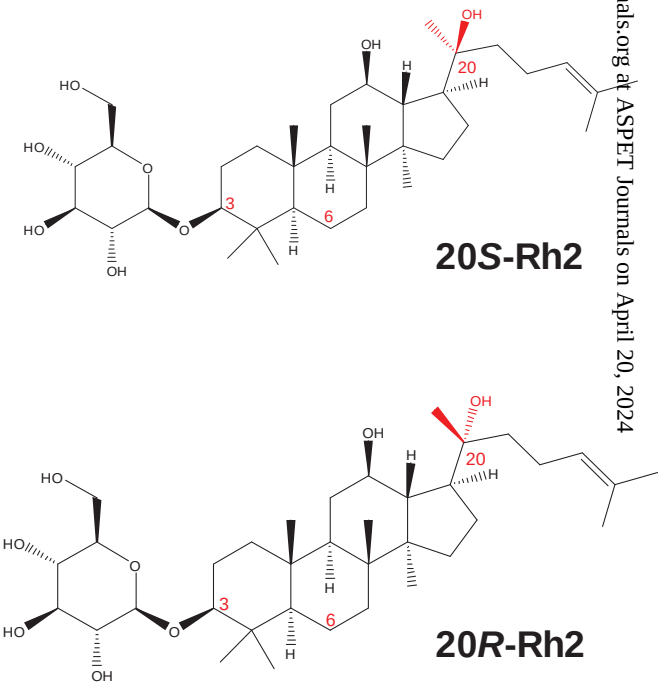

Figure 6

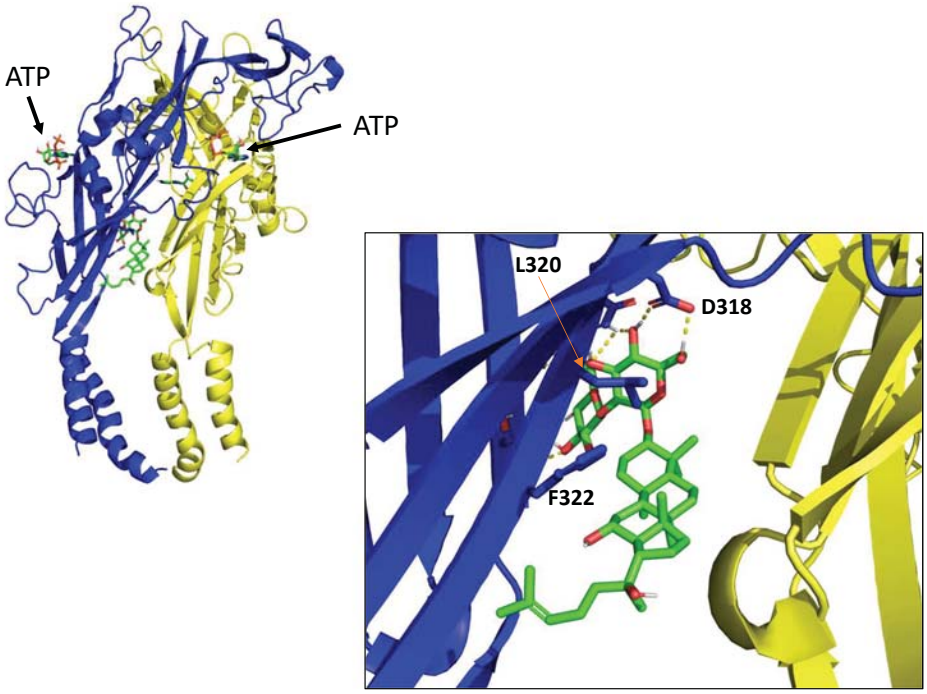

Figure 7

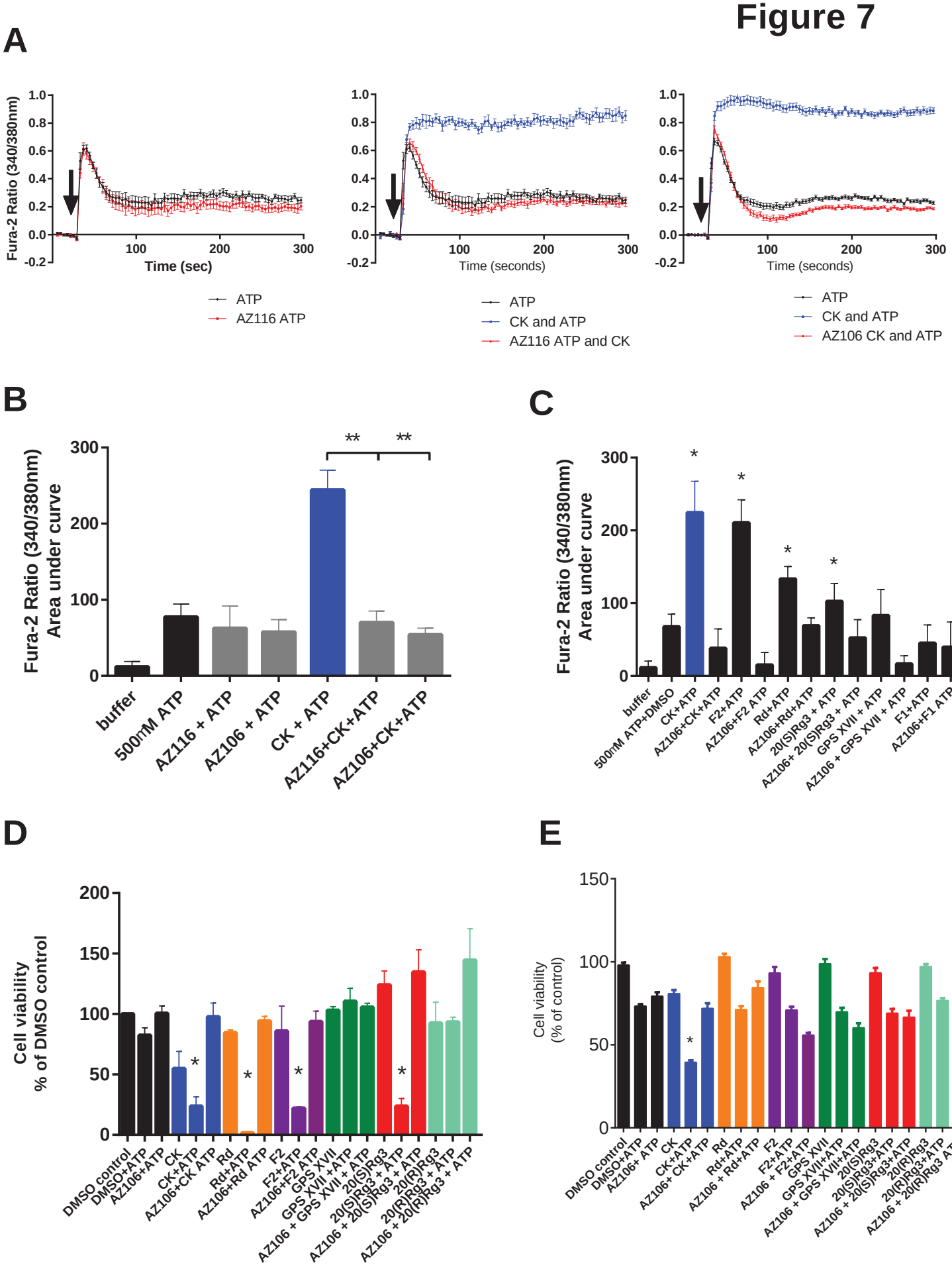

Figure 8

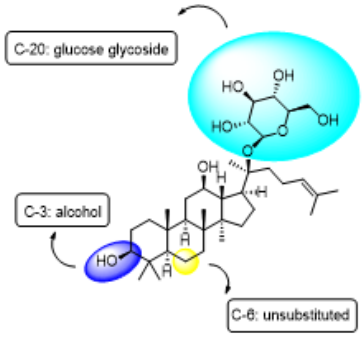

Ginsenoside CK

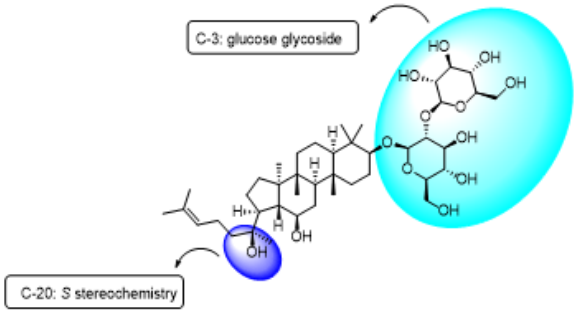

Ginsenoside (20*S*)-Rg3

Supplemental Information: MOLPHARM-AR-2020-000129

Insights into the structure-activity relationship of glycosides as positive allosteric modulators acting on P2X7 receptors

Waraporn Piyasirananda, Andrew Beekman, A. Ganesan, Stefan Bidula, Leanne Stokes

A

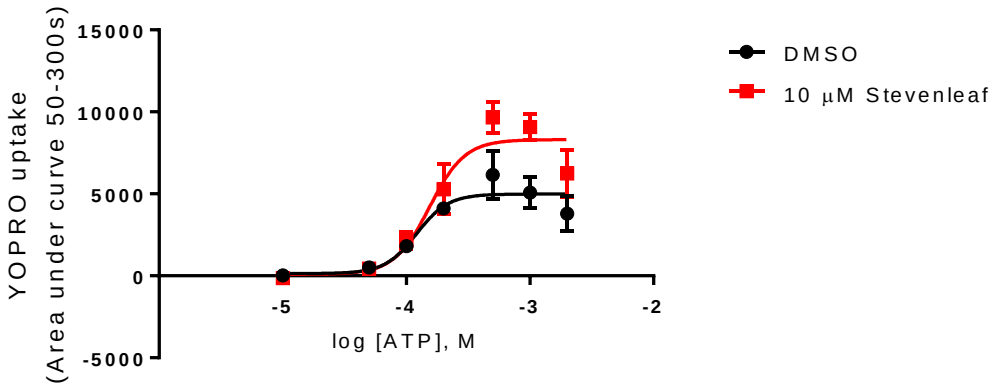

B

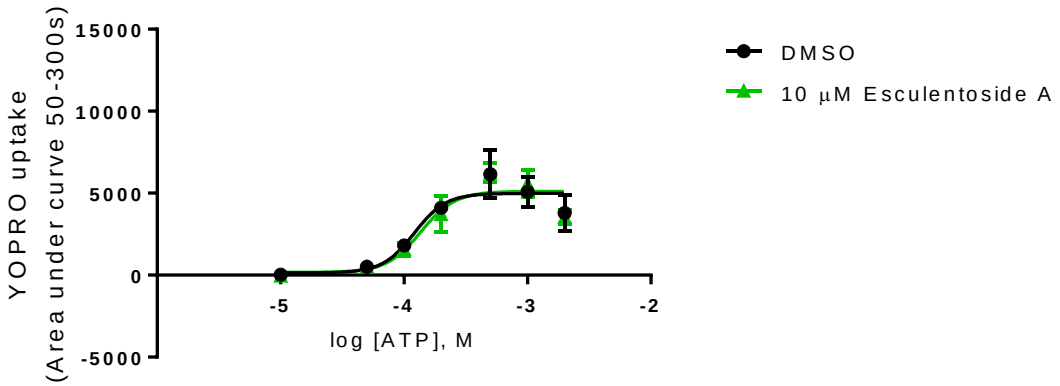

Supplementary Figure 1: Effect of disaccharides stevenleaf and esculentoside A on P2X7. YO-PRO-1 dye uptake was measured in response to ATP in the presence of vehicle (DMSO) or **(A)** stevenleaf (10 µM) or **(B)** esculentoside A (10 µM). Data is collated from three independent experiments and error bars represent standard deviation. Curve fit is a four-parameter non-linear regression performed using GraphPad Prism.

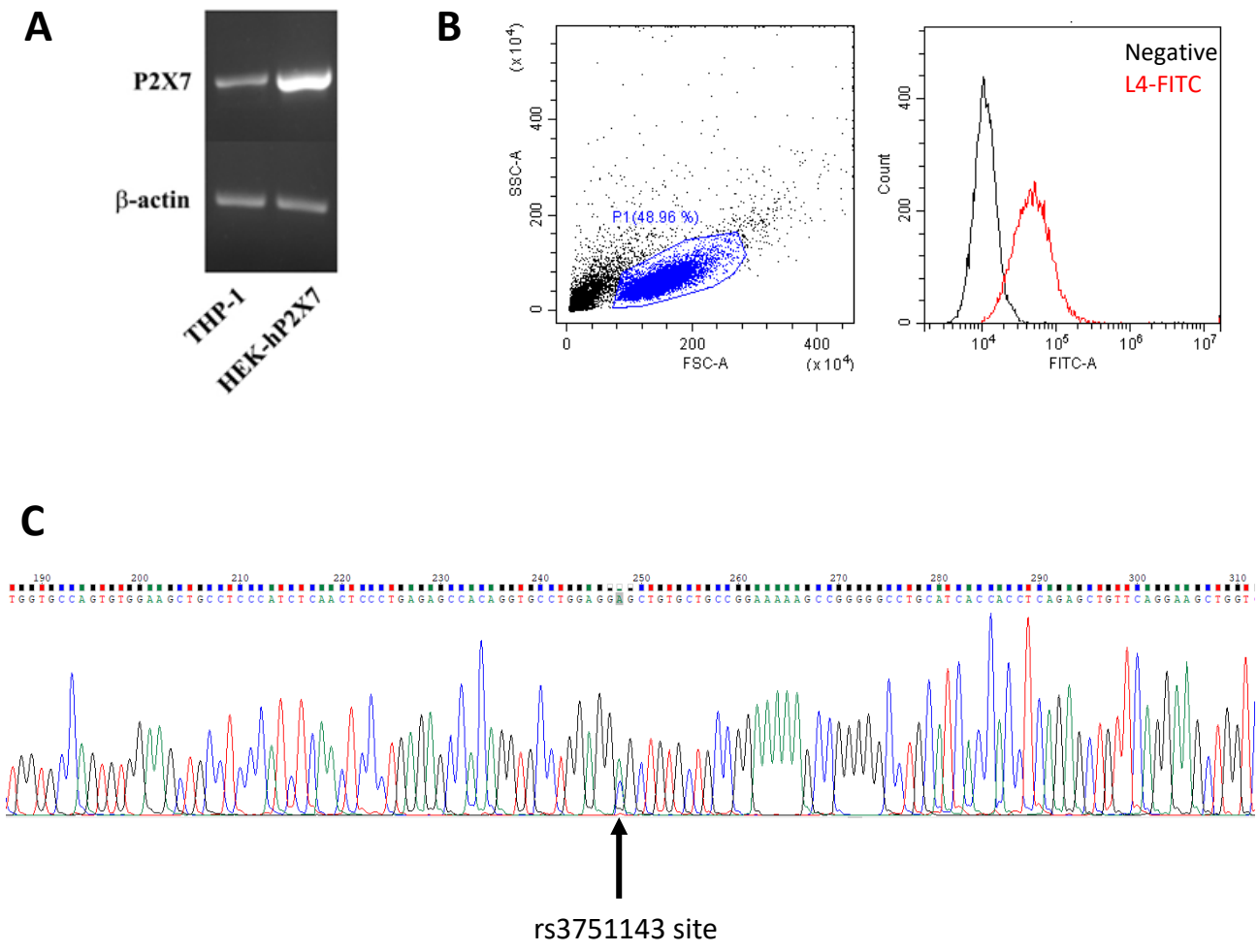

Supplementary Figure 2: P2X7 expression in THP-1 monocytes. (A) RT-PCR was performed to demonstrate P2X7 mRNA expression in THP-1 using HEK-hP2X7 cells as a control. Primer sequences were Forward 5'-CAAAACAGAAGGCCAAGAGC-3' and Reverse 5'-TGCCACATCTGAAAAATTATCG-3' generating a 412bp product. MyTaq Expression of β-actin is shown as a control housekeeping gene. **(B)** Flow cytometry plot showing staining for cell surface P2X7 in THP-1 cells using L4-FITC antibody at 1:100 dilution. **(C)** Sequencing data from P2X7 exon 13 showing two peaks at the rs3751143 site demonstrating the presence of two alleles each containing a different nucleotide (heterozygosity).

Supplemental material: PDB file showing 20(S)-Rg3 docked to a homology model of human P2X7 in the predicted open-state. ATP is also shown within the structure. The model shows the central (most-populated) pose generated using Glide software (Schrodinger suite).